

RESEARCH

Open Access



A network-based approach to overcome BCR::ABL1-independent resistance in chronic myeloid leukemia

Valeria Bica^{1†}, Veronica Venafrà^{1,3†}, Giorgia Massacci², Simone Graziosi¹, Sara Gualdi³, Gessica Minnella^{4,5}, Federica Sorà^{4,5}, Patrizia Chiusolo^{4,5}, Maria Elsa Brunetti⁶, Gennaro Napolitano^{6,7,8}, Massimo Breccia⁹, Dimitrios Mougiakakos^{10,11}, Martin Böttcher^{10,11}, Thomas Fischer^{10,11}, Livia Perfetto^{3*} and Francesca Sacco^{2,6*}

Abstract

Background About 40% of relapsed or non-responder tumors exhibit therapeutic resistance in the absence of a clear genetic cause, suggesting a pivotal role of intracellular communication. A deeper understanding of signaling pathways rewiring occurring in resistant cells is crucial to propose alternative effective strategies for cancer patients.

Methods To achieve this goal, we developed a novel multi-step strategy, which integrates high sensitive mass spectrometry-based phosphoproteomics with network-based analysis. This strategy builds context-specific networks recapitulating the signaling rewiring upon drug treatment in therapy-resistant and sensitive cells.

Results We applied this strategy to elucidate the BCR::ABL1-independent mechanisms that drive relapse upon therapy discontinuation in chronic myeloid leukemia (CML) patients. We built a signaling map, detailing - from receptor to key phenotypes - the molecular mechanisms implicated in the control of proliferation, DNA damage response and inflammation of therapy-resistant cells. In-depth analysis of this map uncovered novel therapeutic vulnerabilities. Functional validation in patient-derived leukemic stem cells revealed a crucial role of acquired FLT3-dependency and its underlying molecular mechanism.

Conclusions In conclusion, our study presents a novel generally applicable strategy and the reposition of FLT3, one of the most frequently mutated drivers of acute leukemia, as a potential therapeutic target for CML relapsed patients.

Keywords Chronic myeloid leukemia, BCR:ABL1-independent resistance, Signaling pathways, Phosphoproteomics, Computational strategy, Drug repurposing, FLT3

[†]Valeria Bica and Veronica Venafrà contributed equally to this work.

*Correspondence:

Livia Perfetto

livia.perfetto@uniroma1.it

Francesca Sacco

francesca.sacco@uniroma2.it

Full list of author information is available at the end of the article



© The Author(s) 2025, corrected publication 2025. **Open Access** This article is licensed under a Creative Commons Attribution-NonCommercial-NoDerivatives 4.0 International License, which permits any non-commercial use, sharing, distribution and reproduction in any medium or format, as long as you give appropriate credit to the original author(s) and the source, provide a link to the Creative Commons licence, and indicate if you modified the licensed material. You do not have permission under this licence to share adapted material derived from this article or parts of it. The images or other third party material in this article are included in the article's Creative Commons licence, unless indicated otherwise in a credit line to the material. If material is not included in the article's Creative Commons licence and your intended use is not permitted by statutory regulation or exceeds the permitted use, you will need to obtain permission directly from the copyright holder. To view a copy of this licence, visit <http://creativecommons.org/licenses/by-nc-nd/4.0/>.

Background

Chronic Myeloid Leukemia (CML) is a clonal myeloproliferative disorder, molecularly defined by the presence of the Philadelphia chromosome, resulting from a reciprocal translocation between chromosomes 9 and 22 [t(9;22)(q34;q11)] [1]. This translocation leads to the formation of the BCR::ABL1 chimeric protein, a constitutively active tyrosine kinase that drives aberrant proliferation and survival, promoting leukemogenesis [2]. Given the pivotal role of BCR::ABL1 in CML pathogenesis, tyrosine kinase inhibitors (TKIs), such as imatinib, were developed, markedly improving patient survival [3, 4]. However, TKI therapy fails in about 30% of newly diagnosed CML patients, due to different mechanisms of resistance [5]. TKI resistance mechanisms can be broadly classified as BCR::ABL1-dependent or BCR::ABL1-independent [6]. CML non-responder patients with BCR::ABL1-dependent resistance are typically characterized by the acquisition of point mutations in the kinase domain or overexpression of the oncogene [7] and can receive specific TKIs according to mutational assessment. In contrast, 50% or more of non-responder patients do not harbour BCR::ABL1 mutations and lack therapeutic strategies, as the basis of such BCR::ABL1-independent resistance remains poorly understood [8–10]. BCR::ABL1 independent resistance mechanisms also play a crucial role in leukemia stem cells (LSCs), which are intrinsically resistant to TKI therapy and hinder long-term discontinuation, namely treatment-free-remission, in responder patients [11, 12]. In our study, we aim to elucidate the BCR::ABL1-dependent and -independent resistance mechanisms, with the ultimate goal of proposing novel therapeutic strategies to counteract resistance and improve clinical outcomes of relapsed or unresponsive CML patients. To achieve this, we developed and applied a novel, generally applicable strategy combining high-sensitive mass spectrometry (MS)-based (phospho) proteomics with novel computational algorithms. By this strategy, we first derived two comprehensive BCR::ABL1-dependent and BCR::ABL1-independent signaling maps, identifying novel players in imatinib response and deciphering the complex signaling pathways rewiring occurring in CML resistant cells. Next, by integrating these two maps with the *Druggability Score* algorithm, we identified and validated promising drug targets killing resistant cells. Ex vivo validation in LSCs highlighted a crucial role of acquired FLT3-dependency in resistant CML models. Finally, our study provides insights into the mechanisms underlying imatinib response and resistance and identifies FLT3-TKIs e.g. midostaurin as a potential effective therapeutic strategy for unresponsive patients.

Methods

Cell culture

K562 cell line was provided by courtesy of professor D. Barilà. LAMA84 cell line was obtained from DSMZ. K562-R cells were generated by exposure of K562 cells to increasingly higher concentration of imatinib during a period of several weeks. The cells were cultured in RPMI 1640 medium (Hyclone, Thermo Scientific, Waltham, MA) supplemented with 10% heat-inactivated fetal bovine serum (ECS0090D Euroclone, Italy, MI), 100 U/ml penicillin and 100 mg/ml streptomycin (Gibco 15140122), 1 mM sodium pyruvate (Sigma-Aldrich, St. Louis, Missouri, United States, S8636) and 10 mM 4-(2-hydroxyethyl)-1-piperazineethanesulfonic acid (HEPES) (Sigma H0887). Responders and non-responder patients derived primary blasts mRNA were provided by courtesy of professor P. Chiusolo.

Immunoblot analysis

K562 and K562-R cells were seeded at a concentration of 500,000 cells/ml and treated as indicated. After treatments cells were centrifuged and washed in ice-cold PBS 1x. Next, cells were lysed in ice-cold RIPA lysis buffer (150 mM NaCl, 50 mM Tris-HCl, pH 7.5, 1% Nonidet P-40, 1 mM EGTA, 5 mM MgCl₂, and 0.1% SDS) supplemented with 1 mM PMSE, 1 mM orthovanadate, 1 mM NaF, protease inhibitor mixture 1x, inhibitor phosphatase mixture II 1x, and inhibitor phosphatase mixture III 1x and incubated for 30 min. Samples were centrifuged at 13,000g for 30 min and supernatants were collected. The total protein concentration was determined using the Bradford reagent (Biorad, 5000006). Protein extracts were denatured and heated at 95 °C for 10 min in NuPAGE LDS Sample Buffer (Thermo Fisher Scientific, NP0007) and DTT as a reducing agent (NuPAGE Sample Reducing Agent) (Thermo Fisher Scientific, NP0004). Denatured proteins were resolved using 4–15% Bio-Rad Mini-PROTEAN TGX/CRITERION polyacrylamide gels (Bio-Rad 4561084). Proteins were transferred to Trans-Blot Turbo Mini Nitrocellulose Membranes using a Trans-Blot Turbo Transfer System (Bio-Rad, 17001918). The nitrocellulose membranes were incubated in blocking solution (5% BSA, 0.1% Tween 20 in TBS 1x) at room temperature for 1 h. Saturated membranes were incubated overnight with primary antibodies (Table C) diluted in 5% BSA or 5% skimmed milk powder, depending on manufacturer instruction. HRP-conjugated secondary antibodies (Goat Anti-Mouse IgG (H+L)-HRP Conjugate 1:3000, BIORAD 1721011) were diluted in 5% skimmed milk powder, 0.1% Tween 20 in 1x TBS and used for the detection of the primary antibodies. Chemiluminescence was detected using Clarity Western ECL Blotting Substrates (Bio-Rad) and the Chemidoc (Bio-Rad). Band densities

were quantified using ImageJ and normalized to the loading control.

Cell cycle analysis

Cells were treated with imatinib for 24 h at a concentration of 500.000 cell/ml. The following day 10^6 cells were collected from each sample and washed with ice-cold PBS. Cells were resuspended in 1 $\mu\text{g/ml}$ DAPI (Thermo Scientific, #62248) and 0.2 mg/ml RNase (Thermo Scientific, #12091021) PBS solution and incubated for 30 min before flow cytometry analysis. The fluorescence intensity was detected using CytoFLEX S (Beckman Coulter). Fluorescence intensity was measured using a CytoFLEX S instrument (Beckman Coulter). Weekly quality control checks for the cytometer were performed using CytoFLEX Daily QC Fluorospheres (Beckman Coulter B53230). Data acquisition was conducted using CytExpert software (Beckman Coulter).

MTT assay

Cell viability was measured using the Cell Proliferation Kit I (MTT) (Roche, 11465007001). Cells were treated with drugs reported on **Table B** for 24 h at a concentration of 50.000 cells/ml or 72 h at a concentration of 10.000 cells/ml. 100 μl of cell suspension were seeded in technical triplicate in a 96 multiwell plate. After 24 h of treatment, 10 μl of MTT were added to the cells and incubated for 4 h at 37 °C. Solubilization Buffer was used to dissolve the formazan crystals during an overnight incubation. Finally, the plates were read at 595 nm using a microplate reader (Bio-Rad).

Real time quantitative PCR

$5 \cdot 10^6$ cells were centrifuged and resuspended in 1 ml Trizol reagent (Thermo Fisher Scientific). After 5 minutes incubation at room temperature, 200 μl of ice-cold chloroform and vigorously shaken for 15 seconds. Samples were centrifuged at 12000 $\times\text{g}$ for 15 minutes and aqueous supernatant containing RNA were collected. Next samples were added with 500 μl isopropanol and 10 μg of glycogen and incubated overnight at -20°C. The following day samples were centrifuged at 12000 $\times\text{g}$ for 10 minutes and supernatant was discarded. Pellets were washed with 1 ml ice-cold ethanol 75% and centrifuged again at 7500 $\times\text{g}$ for 5 minutes. Ethanol was allowed to evaporate and pellets were resuspended in RNase free water. Quantification and purity of the samples was determined with NanoDrop Lite (Thermo Scientific). 1000 ng of RNA from each sample underwent retrotranscription. PrimeScript RT reagent Kit (Takara) was used following manufacturer's instructions. Specific primers for the BCR::ABL1 gene were designed (forward: 5'-TGACCAACTCGTGTGTGAAACTC-3'; reverse: 5'-TGACCAACTCGTGTGTGAAACTC-3'). RT-qPCR was performed using the SYBR

Premix Ex Taq (Takara) kit and the QuantStudio[®]3 Real-Time PCR instrument (Applied Biosystems). The fold changes in mRNA levels were normalized on actin gene expression. The comparative analysis of gene expression was evaluated by expressing the values as $\text{Log}_{10}2^{-\Delta\text{Cq}}$.

Immunofluorescence analysis

To assess γH2AX modulation upon 1 μM imatinib 24 h treatment, $5 \cdot 10^6$ cells were treated as indicated, washed in PBS and fixed in 4% PFA for 30 min. Next, cells were washed in PBS and permeabilized in a PBS + 0,1% Triton solution for 10 min. After the incubation time, cells were centrifuged at 6000 $\times\text{g}$ for 5 min, washed in PBS and centrifuged again at 10.000 $\times\text{g}$ for 5 min. Cells were blocked in a PBS + 2% BSA + 0,01% Tween20 solution for 1 h and then centrifuged at 10.000 $\times\text{g}$ for 5 min. Cells were incubated with γH2AX primary antibody (CST 9718) for 1 h and washed three times in PBS + 0,01% Tween20. Next, cells were incubated with secondary antibody (Southern-Biotech 4050-30) for 1 h and washed three times. Cells were stained with DAPI (Thermo Scientific #62248) for 15 min, centrifuged at 6000 $\times\text{g}$ for 5 min and mounted for imaging. The experiment was performed in biological triplicate. Samples were quantified considering the percentage of γH2AX -positive cells (>5 γH2AX foci) over the total number of cells.

Sample Preparation for proteomic and phosphoproteomic analysis

Cells were lysed in SDC lysis buffer added with 4% (w/v) SDC, 100 mM Tris -HCl (pH 8.5). Next, samples were boiled at 95° for 5 min and sonicated in Bioruptor for 10 cycles at high intensity 30s on/30s off. Protein concentration was determined by BCA assay. inStageTip (iST) method was used for proteome preparation [13]. Briefly, 50 μg of protein extract were diluted in 2% SDC buffer and 1% trifluoroacetic acid (TFA). SDBRPS tips were washed with (i) 100 μl acetonitrile (ACN), (ii) 100 μl of 30% methanol and 1% TFA and (iii) 150 μl of 0.2% TFA by centrifuging tips at 1000 $\times\text{g}$ for 3 min. Samples were loaded onto equilibrated columns and spin at 1000 $\times\text{g}$ for 10 min. SDBRPS tips were washed with (i) 100 μl of 1% TFA in ethyl acetate, (ii) 100 μl of 1% TFA in isopropanol and (iii) 0.2% TFA. For protein elution, we used a buffer containing 80% ACN, 5% NH_4OH in MilliQ water. Samples were centrifuged at 1000 $\times\text{g}$ for 4 min and concentrated by SpeedVac at 45° for ~45 min. Finally, samples were resuspended in 10 μl of a buffer added with 2% ACN and 0.1% TFA. EasyPhos workflow was used to prepare phosphoproteomics samples as previously described [14]. Briefly, at least 750 μg of protein extract was diluted in 750 μl of ACN and 250 μl of EP enrichment buffer added with 36% TFA and 3mM KH_2PO_4 . Samples were mixed at 2000 $\times\text{g}$ for 30 s to clear precipitates, then

centrifuged at 20,000 xg for 15 min and finally transferred in a 2 ml deep-well plate. TiO₂ beads were used. For each sample, 12:1 (beads: protein) were weighed out and resuspended in EP loading buffer additioned with 80% ACN and 6% (v/v) TFA. Activated TiO₂ beads were added to each sample and incubated for 5 min at 40° C at 2000 rpm. Next, beads were centrifuged at 2000 xg for 1 min and supernatants (non-phosphosites) were discarded. The beads were resuspended in 500 µl of EP wash buffer, composed of 60% ACN and 1% TFA twice and then transferred to a clean tube/plate. Four additional washes with EP wash buffer were carried out mixing at 2000 rpm for 3 s. Following the wash steps, the beads were resuspended in 75 µl of EP transfer buffer (80% ACN, 0.5% acetic acid), transferred onto C8 stage tips (double layer), and spun to dryness at 1000 xg for 5 min. Phosphopeptides were eluted in 30 µl of EP elution buffer containing 200 µl of NH₄OH and 800 µl of 40% ACN into PCR tubes. Immediately afterward, the samples were concentrated in a SpeedVac at 45 °C for 20 min. Meanwhile, SDBRPS tips (triple layer) were equilibrated using the following steps: (i) 100 µl ACN, (ii) 100 µl 30% methanol and 1% TFA, and (iii) 150 µl 0.2% TFA. After completion of the SpeedVac, SDBRPS loading buffer (1% TFA in isopropanol) was added to the samples. Subsequently, phosphopeptides were loaded onto equilibrated SDBRPS StageTips and washed sequentially with (i) 100 µl 1% TFA in ethyl acetate (EtOAc), (ii) 100 µl of 1% TFA in isopropanol, and (iii) 150 µl of 0.2% TFA. After the wash steps, phosphopeptides were eluted into clean PCR tubes using a buffer containing 60% ACN and 5% NH₄OH. Following another SpeedVac step at 45 °C for 30 min, phosphopeptides were resuspended in 10 µl of a buffer containing 2% ACN and 0.1% TFA.

Mass spectrometry analysis

The peptides and phosphopeptides underwent desalting using StageTips and were subsequently separated on a reverse-phase column (50 cm, packed in-house with 1.9-mm C18-Reprosil-AQ Pur reversed-phase beads) (Dr. Maisch GmbH). For single-run proteome analysis, separation occurred over 120 min, while for phosphoproteome analysis, it extended to 140 min. Following elution, the peptides were subjected to electrospray ionization and analyzed via tandem mass spectrometry using an Orbitrap Exploris 480 instrument (Thermo Fisher Scientific). The instrument operated by alternating between a full scan and multiple high-energy collision-induced dissociation (HCD) fragmentation scans, resulting in a total cycle time of up to 1 s.

Proteome and phosphoproteome data processing

Raw files were analyzed using the Spectronaut software. MS/MS spectra were searched against the Homo sapiens

UniProtKB FASTA database (September 2014), with an FDR of <1% at the level of proteins, peptides and modifications. Enzyme specificity was set to trypsin, allowing for cleavage N-terminal to proline and between aspartic acid and proline. The search included cysteine carbamidomethylation as a fixed modification. Variable modifications were set to N-terminal protein acetylation and oxidation of methionine as well as phosphorylation of serine, threonine tyrosine residue (STY) for the phosphoproteomic samples.

Proteome and phosphoproteome bioinformatics data analysis

Bioinformatic analysis was conducted within the Perseus software environment [15], where statistical analysis of both the proteome and phosphoproteome was executed on logarithmized intensities of quantified values across experimental conditions. Normalization of phosphopeptide intensities consisted in subtracting the median intensity of each sample. To identify significantly modulated proteins and phosphopeptides between conditions, a Student t-test with a permutation-based false discovery rate (FDR) cutoff of 0.05 and S0 = 0.1 was employed. Categorical annotation, such as KEGG pathways, was added in Perseus. To address multiple hypothesis testing, a Benjamini-Hochberg FDR threshold of 0.05 was applied.

Imatinib treated K562 and K562-R vs. control network generation with *SignalingProfiler* 2.0

We run the *SignalingProfiler* 2.0 pipeline for K562 cells exposed to imatinib and K562-R cells to generate two networks linking BCR::ABL1 in inactive state (activity = -1) to 9 cancer hallmark phenotypes (Apoptosis, Proliferation, G1/S transition, DNA repair, DNA fragmentation, G1/S transition, Cell cycle block, Cell cycle exit, Autophagy).

Protein activity inference

Proteomic and phospho-proteomic data were processed to make them *SignalingProfiler* 2.0 compliant. Kinase activity was inferred by analyzing the modulation of their target phosphosites between sensitive (resistant) cells and control cells using the *run_footprint_based_analysis* with default parameters. Additionally, regulatory phosphosites' modulation for kinases, transcription factors, and other signaling proteins was considered through the *phosphoscore_computation* function with default parameters. The resulting scores were combined to derive a final activity score. Protein abundance modulation in proteomic data was also considered as a proxy of activity.

For sensitive cells, K562 and LAMA84 multi-omic data were independently exploited to perform *SignalingProfiler* 2.0 protein activity inference step and the two results were merged. We selected 601 proteins that had the same

modulation in the two cell lines. We inferred 244 and 258 kinases, 17 and 22 phosphatases, 214 and 261 transcription factors, and 1684 and 2153 other phosphorylated or modulated in abundance signaling proteins, in imatinib exposed K562 and K562-R cells, respectively.

Network generation

For both cell lines, a signaling network was constructed using *SignalingProfiler* 2.0 prior knowledge network (PKN) with direct interactions. The PKN was filtered to retain only interactions involving proteins quantified in the (phospho)proteomics data using the *preprocess_PKN* function. A naïve network connecting BCR::ABL1 to inferred signaling proteins was generated using the *two_layer_naive_network* with default parameters. Then, to keep in the naïve network only the interactions coherent with the proteins' activity, we applied the *SignalingProfiler* 2.0 two-step multi-shot version of vanillaCARNIVAL optimization [16] with default parameters. The two networks were connected to 9 cancer hallmarks using the *phenoscore_computation* with default parameters. For K562 cells treated with imatinib only interactions from protein to phenotypes coherent with the phenotypic activity were retained using the *optimize_pheno_network* function with default parameters. We generated a network of 200 nodes and 429 edges for K562 cells treated with imatinib and 710 nodes and 1895 edges for K562-R cells. The two networks are available on NDEX (K562: <https://www.ndexbio.org/viewer/networks/e6c7826f-4a6d-11ef-a7fd-005056ae23aa>, K562-R: <https://www.ndexbio.org/viewer/networks/a0c04e02-4a6e-11ef-a7fd-005056ae23aa>).

BCR::ABL1 dependent and independent functional circuits identification

To obtain BCR::ABL1 dependent functional circuit, the *pheno_to_start_circuit* of *SignalingProfiler* (v. 2) R package was used, selecting BCR::ABL1 as a starting node and maximum path length 7. To obtain BCR::ABL1 independent functional circuit, the same function was used selecting 23 receptors with opposite regulation between K562-R and K562 cells or present only in K562-R network, 'Proliferation' and 'Apoptosis' phenotypes as end points and maximum path length 6. The BCR::ABL1 independent functional circuit accounted for 438 nodes and 987 edges. The network is available on NDEX at <https://www.ndexbio.org/viewer/networks/73523fe5-4a6f-11ef-a7fd-005056ae23aa>. For visualization purposes, we selected only paths with maximum path length 5, obtaining a network of 60 nodes and 111 edges. The generated optimized networks were displayed on Cytoscape using the RCy3 package (v. 2.14.2). The 'pheno_layout.xml' XML file provided within the *SignalingProfiler* 2.0 R package was used to set the network style in Cytoscape.

FDA-drug targets for hematological malignancies prioritization

Druggability score

For druggable targets prioritization we exploited the BCR::ABL1 independent functional circuit. We first removed nodes with incoherent incoming edges (CARNIVAL activity different than 100 or -100) obtaining a network of 424 and 875 edges. For each node, we computed a *topology score* considering: the network degree (i), the number of paths (maximum length = 10) inhibiting apoptosis (ii) and activating proliferation (iii). To not take into account indirect interactions, for each node we excluded paths with length 1, when longer paths were present. Each score was loghartimized and normalized between 0 and 1 and the average was computed (*topology score*). The *topology score* of each node was multiplied with the *CARNIVAL activity score* of the normalized between -1 and 1, obtaining the *Druggability Score*. Proteins with a positive *Druggability Score* are expected to induce more cell death in K562-R cells than in control cells. In contrast, proteins with a negative *Druggability Score* should exhibit the opposite effect. To identify the FDA-approved drug targets for hematological malignancies we manually associated to the drugs of [16] the Primary Gene Name of the molecular target (*FDA-drug targets catalogue*) and 13 network nodes were extracted.

In vitro validation

For in vitro validation, we selected 8 network nodes (BCL2, JAK1, BTK, FLT3, PI3KCB and PI3KC3, DNMT1 and DNMT3A) that had a positive *Druggability Score* and that were present in the FDA-drug targets catalogue. As a negative control, we also considered AKT1 node that had a negative *Druggability Score*. MTT viability assay was performed treating K562 and K562-R for 24 h with inhibitors reported in **Table B**. For each cell line the half maximal inhibitory concentration (IC50) was computed using IC50 calculator web tool (AAT Bioquest) and the opposite of logarithm was computed and compared with the *Druggability Score*.

Analysis of drug sensitivity of primary CML bone marrow samples

For drug sensitivity testing of primary patient material, bone marrow mononuclear cells (MNCs) from 3 different patients were used. Patient samples were collected in accordance with the Declaration of Helsinki, following informed consent. MNCs were thawed from a biobank and stained for cell sorting using CD45-PE/Cy7 (Biolegend, clone 2D1), CD34-BV510 (Biolegend, clone 581), CD38-BV785 (Biolegend, clone HIT2), and CD26-FITC (Biolegend, clone BA5b). Leukemic progenitor cells (LPCs, CD38 high /CD26 dim) and leukemic stem cells (LSCs, CD38 dim /CD26 high) were sorted (Fig. S4).

Samples were cultured for 24 h in the absence or presence of midostaurin 300nM at 37 °C, 5% CO₂, and subsequently analyzed using a CytoSMART™ automated cell counter (Corning), including Trypan Blue-based live/dead discrimination.

CML patients RNA-seq analysis

RNA was extracted from peripheral blasts of 3 imatinib responder and 4 non responder CML patients (Table S8). Samples were obtained upon the patients' informed consent. Briefly, RNA was prepared from PBMCs using the RNeasy Mini Kit (QIAGEN, Germany). The pellets obtained from buffycoat were resuspended in the RLT buffer. We proceed with the addition of equal volume of 70% Ethanol (EtOH) to our already homogenized sample in RTL. It was spinned at $\geq 8000 \times g$ for 15 s. 700 μ l of Buffer RW1 were added and the solution was spinned at $\geq 8000 \times g$ for 15 s. It was emptied carefully, and 500 μ l of RPE Buffer were added and the solution was spinned $\geq 8000 \times g$ for 2 min. The column was emptied again and placed in a new tube and centrifuged at maximum power for 1 min to dry.

Library construction protocol	NEGEDIA Digital mRNA-seq research grade sequencing service 2.0 (Next Generation Diagnostic srl)
Library strategy	NEGEDIA Digital mRNA-seq v2.0
Data processing step	Illumina Nova Seq 6000 base call (BCL) files were converted in fastq file through bcl2fastq (v2.20.0.422). Data was processed using nf-core/rnaseq v3.14.0 [17] of the nf-core collection of workflows [18], utilizing reproducible software environments from the Bioconda [19] and Biocontainers [20] projects. The pipeline was executed with Nextflow v23.10.1 [21].

NFkB targets analysis

The RNAseq analysis of LSCs and LPCs from 5 CML patients from the GEO database (GSE43754) was conducted within the Perseus software environment [15]. To identify significantly modulated transcripts, a one sample Student t test with a permutation-based false discovery rate (FDR) cutoff of 0.07 and $S_0 = 0.1$ was employed. To address multiple hypothesis testing, a Benjamini-Hochberg FDR threshold of 0.05 was applied. To analyze the modulation of NFKB1 targets, we selected NFKB1 regulon in *SignalingProfiler* (v. 2.0) database combining SIGNOR and CollecTRI [22] information. We merged the NFKB1 regulon with significantly modulated transcripts with an absolute fold-change higher than 1. The fold-change in each patient is reported in Fig. 6C.

Statistics

All experiments were independently replicated at least three times ($n = 3$). Data are expressed as

means \pm standard error (SEM). When comparing three or more groups, statistical analyses were conducted using either one-way or two-way analysis of variance (ANOVA). For comparisons between two groups, the unpaired t-test was employed, assuming a two-tailed distribution. Statistical significance was defined as follows: * $p < 0.05$; ** $p < 0.01$; *** $p < 0.001$. Prism 7 (GraphPad) was utilized for all statistical analyses.

Results

The experimental strategy

To characterize the BCR::ABL1 independent signaling pathways and identify novel druggable targets, we developed an innovative multi-step strategy, which can be broadly applied to propose novel effective therapeutic strategies in cancer cells exhibiting therapeutic resistance in absence of clear genetic alterations. Below is a step-by-step description of our strategy (Fig. 1A):

Step 1. Use MS-based (phospho)proteomics to in depth characterize the signaling pathways remodeling induced in therapy-resistant and sensitive cancer cells upon drug treatment.

Step 2. Leverage the network-based computational algorithm *SignalingProfiler* 2.0 [23] to analyze the newly generated phosphoproteomic dataset and obtain two signaling maps describing the molecular mechanisms underlying the drug response in therapy-resistant and sensitive cancer cells. By this step, we obtained two signaling maps detailing the BCR::ABL1-dependent (imatinib-treated sensitive cells vs. untreated sensitive cells) and -independent (untreated sensitive cells vs. untreated resistant cells) signaling pathways.

Step3. Employ the *Druggability Score* algorithm to identify and prioritize druggable nodes in the resistant signaling map based on their activation levels in therapy-resistant cells and their centrality within the network map. In this step, FDA-approved drugs may be repurposed to eradicate resistant cells.

Step4. Validate the functional role of the top-ranking druggable nodes by treating therapy-resistant cancer cells with small molecule inhibitors targeting these nodes and assessing their viability. In our study, the functional significance of the druggable nodes was validated in CML cell lines and patient-derived leukemic stem cells.

In our study, as a first step, we established a CML cell line model exhibiting imatinib resistance due to BCR::ABL1-independent mechanisms. Specifically, upon chronic imatinib exposure of K562 cells, we selected a persistent clone (K562-R) (Fig. 1B). Notably, the persistence of these cells is accompanied by a drastic reduction of the BCR::ABL1 expression level and inactivation of its downstream proteins (Fig. 1C-D, S3F), without any impact on their cell cycle progression (Fig. 1E). Thus, K562-R cells exhibit BCR::ABL1-independent signaling

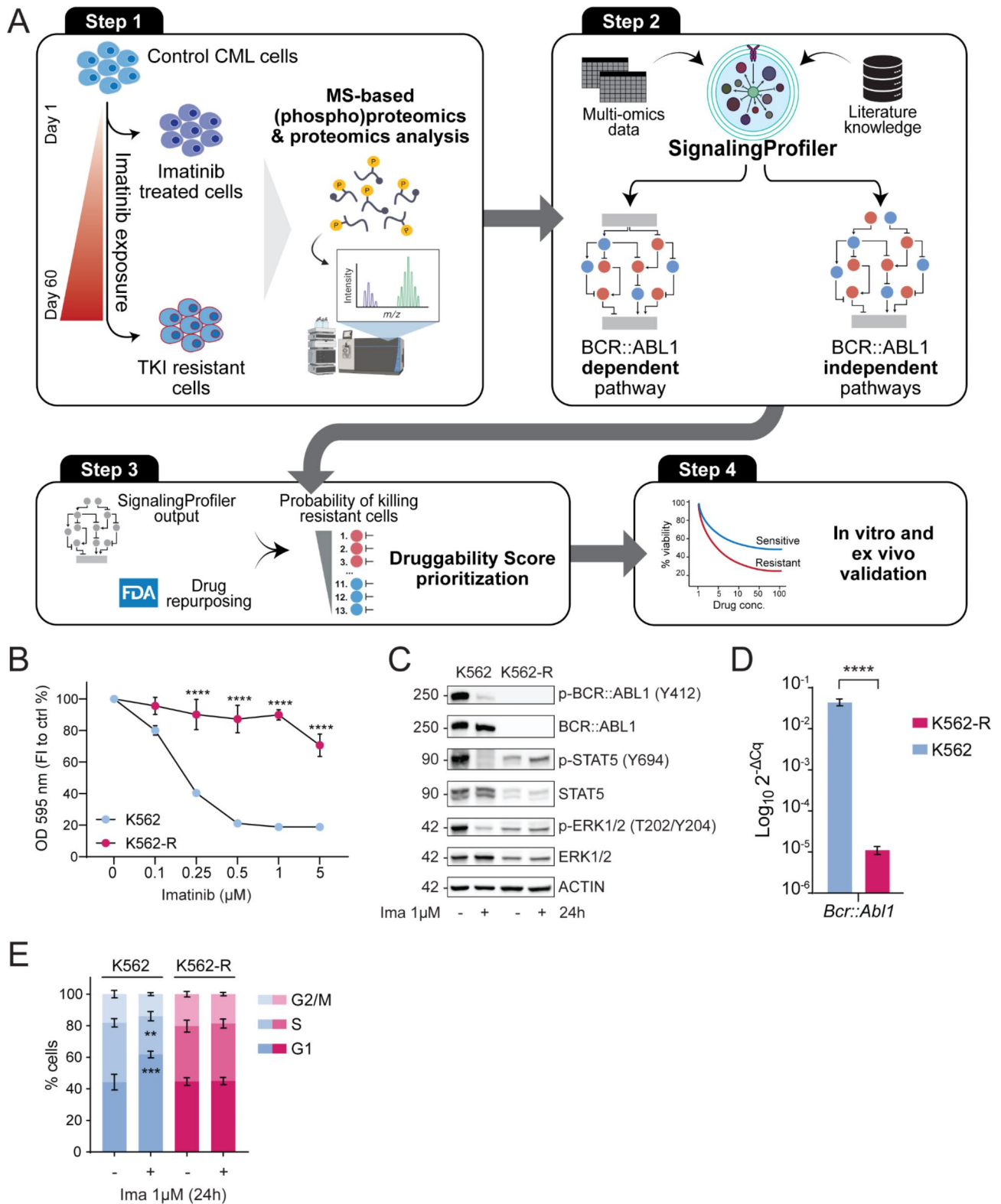


Fig. 1 (See legend on next page.)

(See figure on previous page.)

Fig. 1 Experimental strategy and in vitro resistant model characterization. **A.** Schematic representation of the multi-step strategy. **B.** MTT viability assay. Sensitive cells (blue) and resistant cells (red) were exposed to increasing concentration of imatinib (0.1 μM , 0.25 μM , 0.5 μM , 1 μM and 5 μM) for 72 hours. The graph shows the percentage of absorbance at 595 nm normalized on control condition. **C.** Representative western blots of BCR::ABL1 activity status (Y412), MAPK and JAK/STAT canonical downstream pathways (p-STAT5 (Y694), p-ERK1/2 (T202/Y204)) in K562 and K562-R cells upon 24 h of 1 μM imatinib treatment. **D.** Real Time quantitative PCR was performed to measure BCR::ABL1 transcript levels in K562 and K562-R cells. Bar graph shows quantification of the BCR::ABL1 mRNA levels as $\text{Log}_{10}2^{-\Delta\Delta\text{Ct}}$. **E.** Flow cytometry analysis of cell cycle progression of K562 and K562-R cells upon 24 h exposure to imatinib 1 μM . The bar graph shows the percentage of cells in a specific cell cycle phase measured using DAPI staining

pathways promoting cell survival and can be used as an experimental model to study non-genetic mechanisms driving relapse in CML patients.

In depth phosphoproteomic analysis of Imatinib sensitive and resistant CML cells

The first step of our strategy involves the characterization of the phosphoproteome profile of therapy-resistant and sensitive cells. Thus, state-of-the-art MS-based (phospho)proteomics was employed to characterize the phosphoproteome of imatinib treated and untreated therapy-sensitive CML cell lines (K562 and LAMA84) and our newly established therapy-resistant CML cell line (K562-R) (Table S1 and S2). By this strategy, more than 7,000 proteins and 19,000 class I phosphosites were quantified in biological quadruplicates (Fig. 2A, Table A). Next, we investigated how the (phospho)proteome was remodelled in imatinib treated and resistant cells, by identifying significantly deregulated proteins and phosphosites using t-test analysis ($\text{FDR} < 0.05$). Specifically, we compared: (i) K562-Ima vs. K562 (control cells), (ii) LAMA84-Ima vs. LAMA84; and (iii) K562-R vs. K562. Imatinib treatment affects approximately 30% of the phosphosites and proteins in K562 and LAMA84 cell lines, while more than 70% of the phosphoproteome and the proteome (15,000 phosphosites and 5,000 proteins) is significantly modulated in therapy-resistant K562-R cells as compared to control cells (Fig. 2A). To note, the impact of imatinib on the (phospho) proteome is highly reproducible in K562 and LAMA84 cell lines ($R = 0.7$), indicating the reliability of our approach (Fig. 2B). Comparison analysis of the proteome and phosphoproteome layers revealed that only 20% of the significantly modulated phosphosites are also consistently changed at the protein level, highlighting the relevance of phosphorylation-based signaling events in driving the imatinib response (Fig. 2C, upper panels). In therapy-resistant K562-R cells, signaling pathways are drastically remodelled compared to control cells. Notably, 60% of the significantly modulated phosphosites are also consistently altered at the protein level (Fig. 2C, bottom panel). Next, we investigated how the proteome and phosphoproteome rewiring in imatinib treated and resistant CML models impacted crucial biological processes by enrichment analysis. Proteins involved in metabolic processes, such as TCA, glycolysis/gluconeogenesis are significantly over-expressed and hyperphosphorylated in both imatinib

treated and resistant cells. Finally, in line with the proapoptotic effect of imatinib, pro-survival, and proliferation signaling pathways, such as JAK/STAT, MAPK, and mTOR, are significantly downregulated through phosphorylation-based mechanisms only in imatinib-treated K562 and LAMA84 cells. Consistently, cell cycle-related proteins are down-regulated only in imatinib-treated sensitive models (Fig. 2D). Taken together, these observations indicate that the imatinib-induced response in LAMA84 and K562 is consistent and robust, and confirm the relevance of our cell lines as models to elucidate the BCR::ABL1-dependent and -independent proliferative pathways.

Characterization of BCR::ABL1-dependent signaling pathways

The second step of our strategy aims to generate two signaling maps detailing the BCR::ABL1-dependent and -independent signaling pathways. To this aim, we analyzed the newly generated phosphoproteomic datasets with the network-based algorithm *SignalingProfiler* 2.0. While in this paragraph we have described how BCR::ABL1-dependent pathways control key biological processes, the next one addresses the BCR::ABL1-independent pathways.

By employing *SignalingProfiler* 2.0, we first inferred the activity of signaling proteins in imatinib-treated K562 and LAMA84 cells as compared to control cells. As detailed in Venafrà et al. [23], protein activity modulation is inferred through two complementary approaches. Footprint-based methods use substrate modulation as a proxy for the activity of upstream kinases or phosphatases. Additionally, the impact of hyperphosphorylation or dephosphorylation on specific protein residues is considered, expanding the analysis beyond kinases/phosphatases to include transcription factors and other phosphorylated proteins. Additionally, in this work, protein abundance was also leveraged as a proxy for activity modulation.

As expected, the treatment similarly impacts the activity of kinases, phosphatases, and transcription factors in K562 and LAMA84 cells ($R = 0.48$, $p = 2.2 \cdot 10^{-16}$) (Fig. S1A, Table S3). Imatinib treatment not only inactivates well-known ABL1 downstream targets (STAT5A, RPS6, CDKs) but also increases the activity of key kinases, such as ATM and NEK family members (e.g., NEK2, NEK5, NEK9), linking DNA damage pathways modulation to

BCR::ABL1 activity. Next, we generated the BCR::ABL1-dependent signaling network. The resulting graph accounts for 200 nodes and 524 edges, suggesting a deep signaling rewiring induced by the drug. Interestingly, the phenotypic inference indicates that imatinib activates apoptosis, DNA fragmentation, autophagy and repair, and inhibits cell cycle progression (e.g., G1/S transition) in both cell lines (Fig. S1B). To reduce the complexity of this map, we selected the functional circuits linking BCR::ABL1 to the predicted phenotypes (Fig. 3A). The network-based approach and the in vitro validation experiments align closely and recapitulate the well-characterized relations between BCR::ABL1 and its downstream signaling pathways (ERK1/2, STAT5 and mTOR), and cell-cycle regulation (Fig. 3B-C, S3A-B). While mTOR and its downstream targets, such as p70S6K, are dephosphorylated and inhibited upon imatinib treatment, feedback loops hyperactivate AKT (Fig. 3B). In line with mTOR pathway inhibition, LC3-II and p62 abundance confirmed an increase in autophagy induction (Fig. 3D, S3E). The inspection of the imatinib-dependent modulation of cell cycle reveals that crucial proteins, including CDKs, Rb, and ATM kinase are significantly and consistently modulated at multiple regulatory layers in cell lines and patients (Fig. 3E) driving G1 phase arrest with consequent inhibition of proliferation, as confirmed by functional assays (Fig. 1E and S1C, S3C). In line with the in silico activation of DNA fragmentation and repair phenotypes, we detected higher γ H2AX levels in imatinib-treated cells (Fig. 3F, S3D). Altogether our data indicate that imatinib-dependent suppression of BCR::ABL1 triggers apoptosis by globally rewiring signaling pathways through DNA damage induction and cell cycle block.

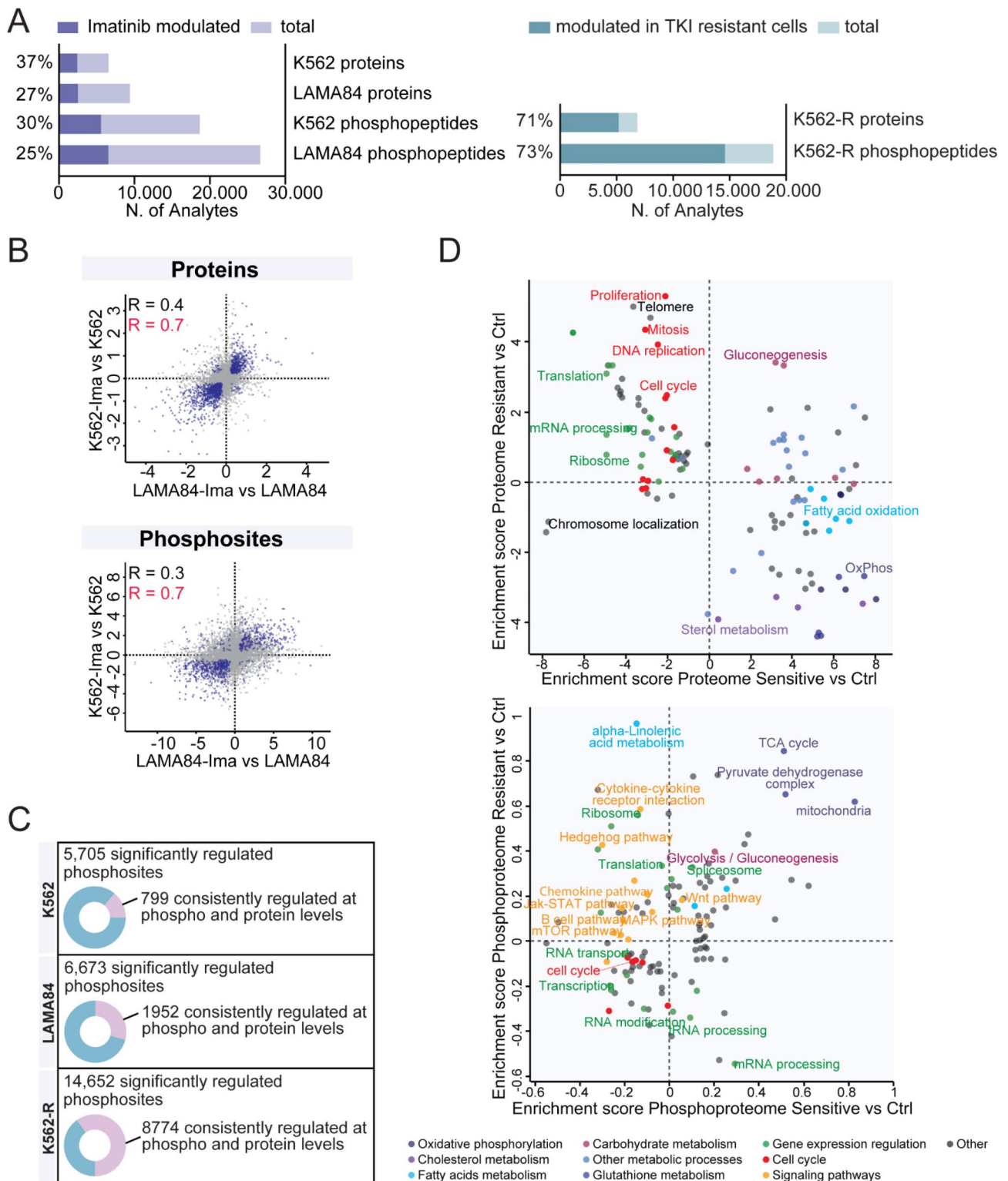
Unbiased identification of BCR::ABL1-independent signaling pathways

Here we aim to obtain a mechanistic picture of the BCR::ABL1-independent signaling remodeling. Thus, we employed our cell line models, namely K562-R and K562-Ima cells, wherein BCR::ABL1 is suppressed, through transcriptional and pharmacological mechanisms, respectively. Interestingly, the two models display divergent behaviour as the first promotes cell survival, whereas the second triggers cell death. This offers the unprecedented opportunity to discover commonly regulated signaling axes, as well as compensative and divergent resistance mechanisms. First, we ran *SignalingProfiler* 2.0 to derive the activity of 261 transcription factors, 280 kinases and phosphatases, and 2153 other signaling proteins in K562-R as compared to control cells (Table S4). As expected, we observe a poor correlation between the inferred activity in resistant cells with respect to imatinib-treated cells (Fig. S2A-B). Most

of the proteins (2470/3005 proteins), including PLK1, LYN, and MYC, are oppositely regulated, supporting the hypothesis that proliferation and survival of K562-R cells rely on BCR::ABL1-independent mechanisms. Next, we employed *SignalingProfiler* 2.0 to derive the K562-R specific network. This resulted in a graph with 700 proteins and 10 phenotypes linked by 1985 interactions, with 20% of phosphorylation events experimentally quantified (Table S4), revealing a huge reorganization in BCR::ABL1-depleted resistant cells. As quality control, we compared our results with genes previously implicated in imatinib resistance by an independent genome-wide CRISPR-Cas9 screening [24]. Remarkably, 70% of the hits are consistently down-regulated and connected in the network (Fig. S2C), supporting the ability of our network-based approach to identify drug resistance pathways. Next, we compared the BCR::ABL1 dependent network with the newly generated K562-R specific map. We observe that BCR::ABL1 downstream signaling effectors, namely STAT5A and CDK1/4, are equally modulated in both models (Fig. S2D), suggesting the persistence of mechanisms associated with the inhibition of BCR::ABL1. To identify BCR::ABL1 independent pro-proliferative molecular mechanisms, we extracted the subnetwork downstream of receptors oppositely modulated in K562-R and imatinib-treated K562 cells (Fig. S2E), and impacting on proliferation and apoptosis (Fig. 4A, Table S5). The BCR::ABL1-independent specific subnetwork as well as validation assays, indicate a complex rewiring of the mTOR pathway. While mTOR is down-regulated, the activity of its canonical targets (e.g. P70S6K) as well as the abundance of the upstream PI3K kinase (p85 α , regulatory subunit) is increased in K562-R as compared to control cells (Fig. 4B, S3G). As revealed by increased activity of BCL2 and inhibition of TP53 and BID, the apoptotic pathway is suppressed. Also, transcription factors MYC and RELA appear consistently regulated by in silico prediction and experimental validation (Fig. 4D-E, S3H). Interestingly, both oncogenic kinases JAK1 and FLT3 are up-regulated at protein and phosphorylation levels (Fig. 4C-F, S3H). Indeed, both FLT3 and JAK1/2 are frequently mutated in haematological disorders and targeted by drugs currently approved in clinics [25]. Taken together, these observations suggest that several signaling proteins, including JAK1 and FLT3, promote cell proliferation in absence of BCR::ABL1, representing promising drug targets.

Repurposing FDA-approved drugs to eradicate resistant CML cells by using the druggability score algorithm

To unbiasedly identify druggable targets killing K562-R cells, we implemented the *Druggability Score* algorithm (Fig. 5A). This method ranks each node within the BCR::ABL1 independent network based on biological



and network topology-based criteria: (i) its activation level in K562-R cells; (ii) its functional relevance for K562-R survival quantified by the number of paths impacting apoptosis and proliferation; (iii) its number

of connections (degree centrality) (Table S6). Proteins with a positive *Druggability Score* are expected to induce greater cell death in resistant cells compared to control cells upon inhibition, whereas proteins with a negative

(See figure on previous page.)

Fig. 2 Phosphoproteomics analysis and functional characterization of sensitive and resistant CML models upon imatinib exposure. **A.** Quantification coverage of phosphopeptides and proteins. For K562 and LAMA84 cells perturbed by 24 h of imatinib 1 μ M treatment, significantly modulated analytes (t test, $S_0=0.1$, $FDR<0.05$) are reported in violet (left panel). For K562-R cells compared to K562 cells, significantly modulated analytes (t test, $S_0=0.1$, $FDR<0.05$) are reported in green (right panel). **B.** Scatterplots showing the Pearson correlation coefficients between the imatinib-dependent changes at the phosphoproteome and proteome levels of K562 cells as compared to LAMA84 cells. Proteins/phosphosites significantly modulated by imatinib, in both K562 and LAMA84 cell lines, are represented in blue. R indicates Pearson correlation considering all proteins/phosphosites (black) or only proteins/phosphosites significantly modulated in both cell lines (red). **C.** Pie charts showing the proportion of phosphopeptides consistently modulated by imatinib (upper panels) or in K562-R cells at their phosphorylation and protein levels. **D.** Scatterplots representing gene ontology enrichment analysis comparing sensitive cells (K562 and LAMA84) upon imatinib treatment with resistant cells (K562-R), at the proteome (upper panel) and phosphoproteome (lower panel) levels

Druggability Score should exhibit opposite effect. Using this approach, we identified 194 and 230 proteins with positive and negative *Druggability Score*, respectively. To prioritize translationally relevant targets, we focused on proteins with FDA-approved inhibitors already in use for hematological malignancies [25], thereby facilitating potential drug repurposing for resistant CML. From the 424 ranked model proteins, we selected eight candidates with positive *Druggability Score* for experimental validation: FLT3, JAK1, BTK, PIK3CB, PIK3C3, DNMT3A, DNMT1, and BCL2 (Fig. 5B). As negative control, we also included AKT, whose *Druggability Score* is negative. FDA-approved inhibitors of these eight proteins were used to treat resistant and sensitive K562 cells, and cell viability was assessed by MTT assay (Fig. 5C). Our in vitro results closely align with the prediction: drugs with a positive *Druggability Score* induce greater cell death in resistant cells as compared to sensitive cells. As expected, pharmacological inhibition of AKT leads to higher cell death in sensitive cells than in resistant ones. Overall, these findings validate the *Druggability Score* as a reliable tool for identifying potential therapeutic targets.

Pharmacological Inhibition of FLT3 kills patient-derived leukemic stem cells

Our in vitro cell viability assay shows that FLT3 inhibition by two different drugs (quizartinib and midostaurin) is the most effective strategy for eradicating resistant CML cells (Fig. S2F). Prompted by these findings, we investigated whether pharmacological suppression of FLT3 could kill leukemic stem cells (LSCs), which are intrinsically resistant to BCR::ABL1 inhibition [26]. LSCs and leukemic progenitor cells (LPCs), isolated from three CML patients, were FACS-sorted (Fig. S4) and treated with midostaurin for 24 h, followed by cell viability assessment. Pharmacological suppression of FLT3 more effectively killed LSCs than LPCs (Fig. 6A, Table S7). In agreement with these results, we found that FLT3 was not only upregulated in K562-R cells at the protein and phosphorylation levels (Fig. 4C), but also at the mRNA level in LSCs as compared to LPCs, as revealed in an independent transcriptome dataset of a cohort of CML patients [27] (Fig. 6B). We next evaluated the FLT3 expression level in a small cohort of six responders

and non responders CML patients. Our analysis indicated that FLT3 expression is elevated in non-responder patients compared to responders, although this difference did not reach statistical significance likely because of the limited cohort size (Fig. S2G). Of note, our results are consistent with a previously published CML patient transcriptome dataset [28] (Fig. S2H). Next, we investigated the molecular mechanisms underlying the FLT3-dependent survival of TKI resistant cells. In depth analysis of our BCR::ABL1-independent network map revealed that FLT3 may drive cell proliferation and survival of TKI resistant cells via NFkB (Fig. 4A), which is predicted to be hyperactivated. Thus, we investigated the role of NFkB in LSCs resistance, by leveraging the transcriptome dataset of LSCs and LPCs derived from five CML patients [27]. As reported in Fig. 6C, NFkB is up-regulated in LSCs, as revealed by the significant over-expression of its target genes, with only one exception. In conclusion, our study reveals that the FLT3-NFkB signaling axis is a driver of the BCR::ABL1-independent resistance, promoting proliferation and survival of leukemic stem cells. Finally, we propose that midostaurin treatment can be an effective alternative strategy for non-responders and relapsed CML patients, which lack BCR::ABL1 genetic alterations (Fig. 6D).

Discussion

Imatinib, known as the “magic bullet”, thanks to its ability to shut-down BCR::ABL1 activity, has revolutionized the treatment landscape of CML. However, tyrosine-kinase inhibitor (TKI) therapy fails in about 30% of newly diagnosed CML patients, which develop different mechanisms of therapy resistance [5]. Additionally, approximately 50% of CML responder patients do not achieve treatment-free remission due to difficulty in completely eradicating LSCs, which are intrinsically resistant to TKIs and are the reservoir for disease persistence [29]. Half of these patients do not show mutations in BCR-ABL1, lacking effective treatment options. This study aims to address that gap. By combining MS-based (phospho)proteomics, *SignalingProfiler*, and a newly developed algorithm (*Druggability Score*), we discovered that resistant leukemic stem cells rely on the activity of FLT3 kinase. These observations pose complex therapeutic questions:

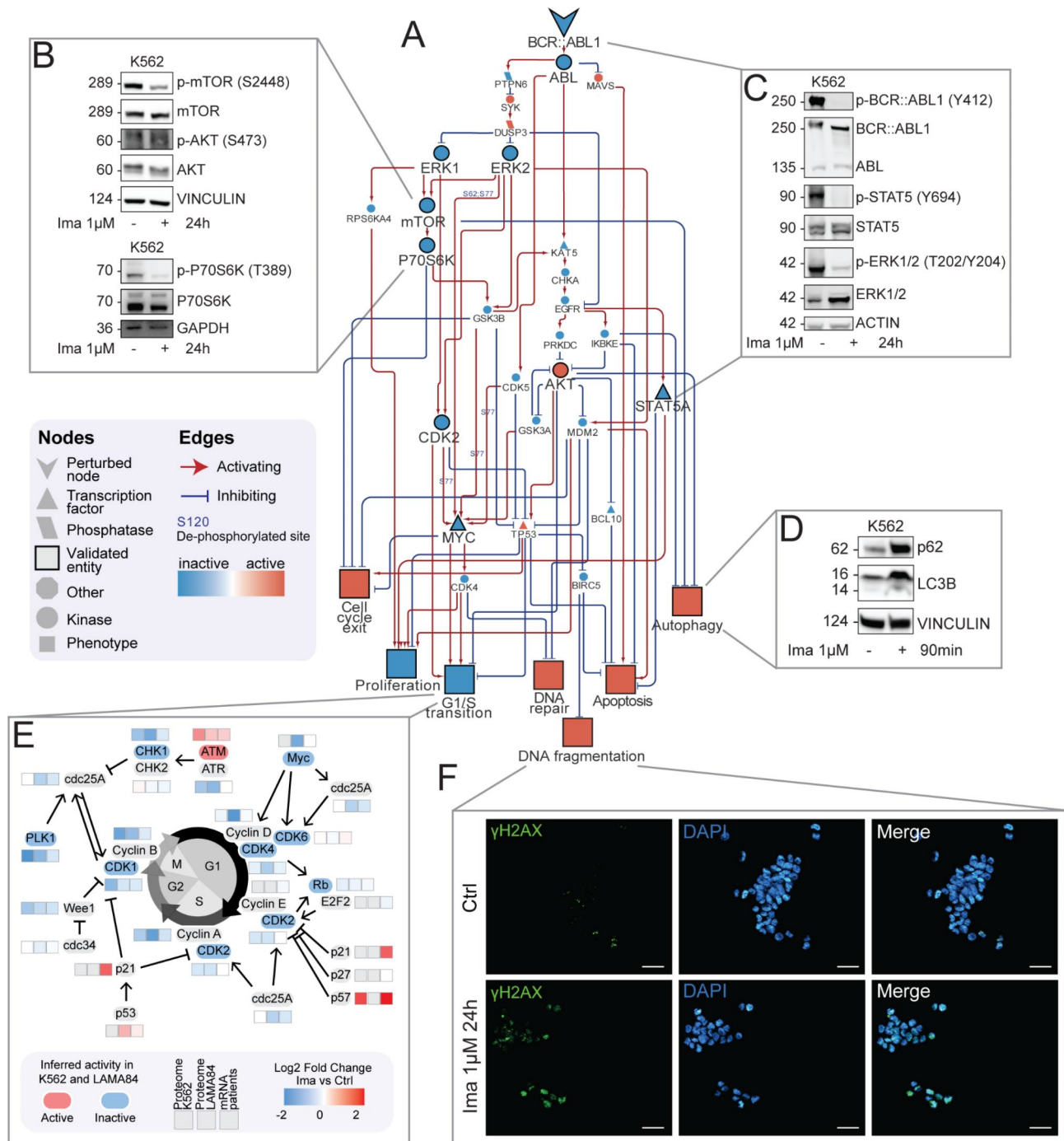


Fig. 3 Characterization of BCR::ABL1-dependent mechanisms in sensitive cells. **A**. Functional submodel extracted from SignalingProfiler 2.0 output linking BCR::ABL1 to cellular phenotypes modulated upon imatinib treatment. **B**. Representative western blots of PI3K/AKT/mTOR axis activity upon 24 h of 1 μM imatinib treatment. **C**. Representative western blots of BCR::ABL1 activity status, MAPK and JAK/STAT canonical downstream pathways upon 24 h of 1 μM imatinib treatment. **D**. Representative western blots showing expression levels of key autophagy regulators, such as p62 and LC3B perturbed by 90 minutes of imatinib 1 μM treatment

for TKI responders, how can we completely eradicate leukemic stem cells? For pan TKI non-responders, what are alternative therapies that can be employed to treat CML? To address these questions, we performed a large-scale integrated analysis, combining state-of-the-art mass

spectrometry-based phosphoproteomics of imatinib responsive and unresponsive cell lines with transcriptomic studies of responsive and unresponsive patient-derived primary blasts and a network-based approach. Hence, we obtained a comprehensive description of the

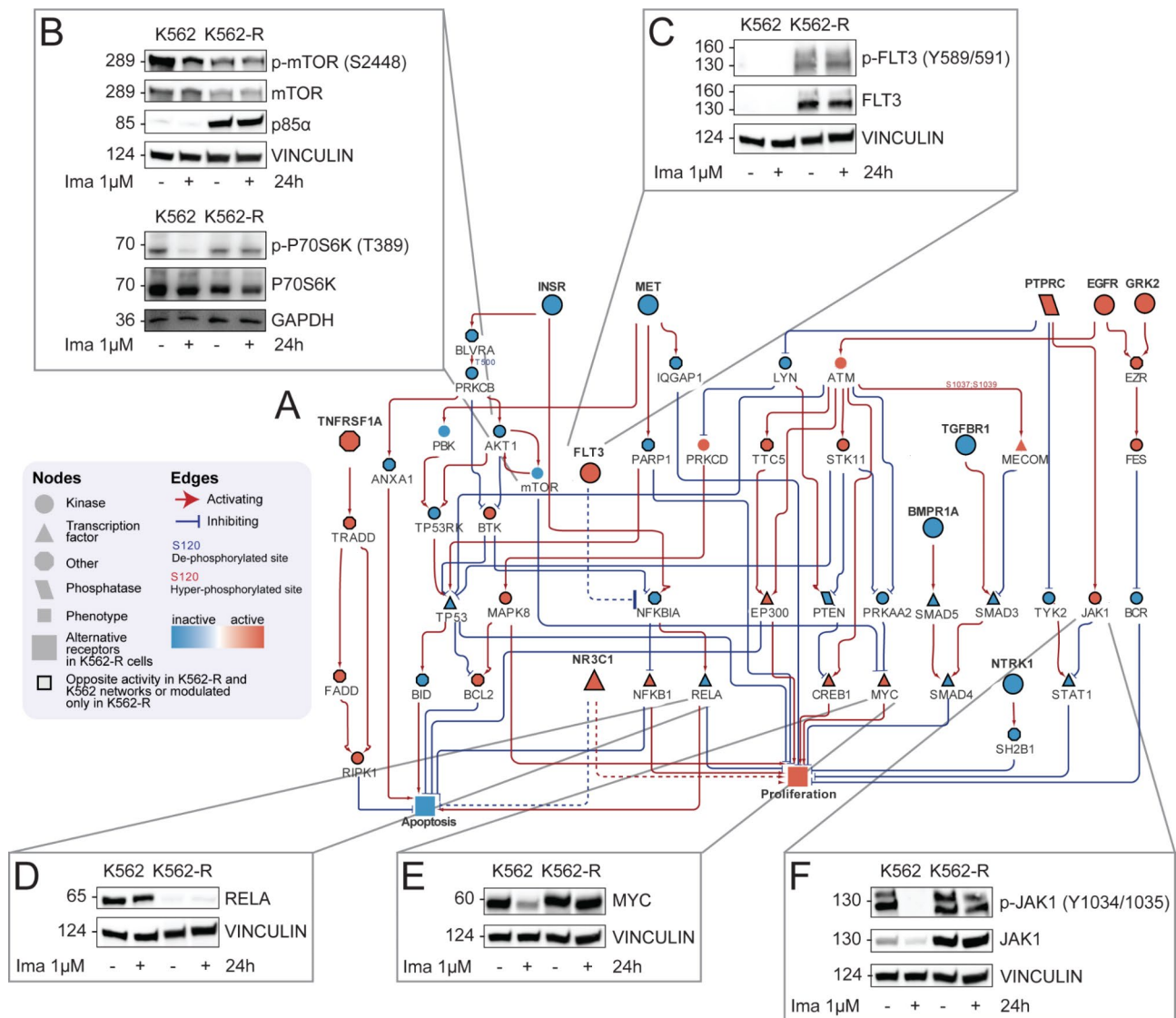


Fig. 4 Characterization of BCR::ABL1-independent mechanisms in resistant cells. **A.** Functional submodel extracted from BCR::ABL1 independent-specific subnetwork reporting paths going from 10 alternative receptors oppositely modulated in imatinib K562-R and K562 cells exposed to imatinib to apoptosis and proliferation phenotypes. **B.** Representative western blots of PI3K/AKT/mTOR axis activity upon 24 h of 1 µM imatinib treatment in control cells and K562-R cells. **C-D.** Representative western blot of control cells and K562-R cells showing phosphorylation status and protein abundance of FLT3 receptor (**C**) and RELA protein (**D**) upon imatinib treatment. Both panels were obtained from the same gel and divided for aesthetic purposes of the figure. **E-F.** Representative western blot of control cells and K562-R cells showing phosphorylation status and protein abundance of MYC transcription factor (**E**) and JAK1 kinase (**F**) upon imatinib treatment. Both panels were obtained from the same gel and divided for aesthetic purposes of the figure

BCR::ABL1 dependent and independent pro-survival signaling mechanisms. With more than 25,000 phosphosites and 8,000 proteins accurately quantified in imatinib treated and resistant cell lines, our large-scale multi-layered dataset represents an unprecedented resource for the scientific community [30, 31]. Imatinib's impact on the global phosphoproteome has been characterized by few studies [32–34]. Consistent with our findings, such datasets revealed that imatinib treatment significantly influences key signaling pathways (e.g., MAPK, JAK/STAT, PI3K/AKT) and crucial biological processes,

including autophagy modulation and DNA damage response.

By employing our in-house implemented *SignalingProfiler* 2.0 pipeline, we derived the molecular paths through which BCR::ABL1 controls crucial phenotypes including cell cycle, autophagy, protein synthesis, and DNA damage [35–38]. Our strategy offered an in-depth description of imatinib-dependent modulation of cell cycle, as most of its regulators were coherently measured at proteome, transcriptome, and activity levels, in cell lines and in patient-derived primary blasts. We acknowledge that

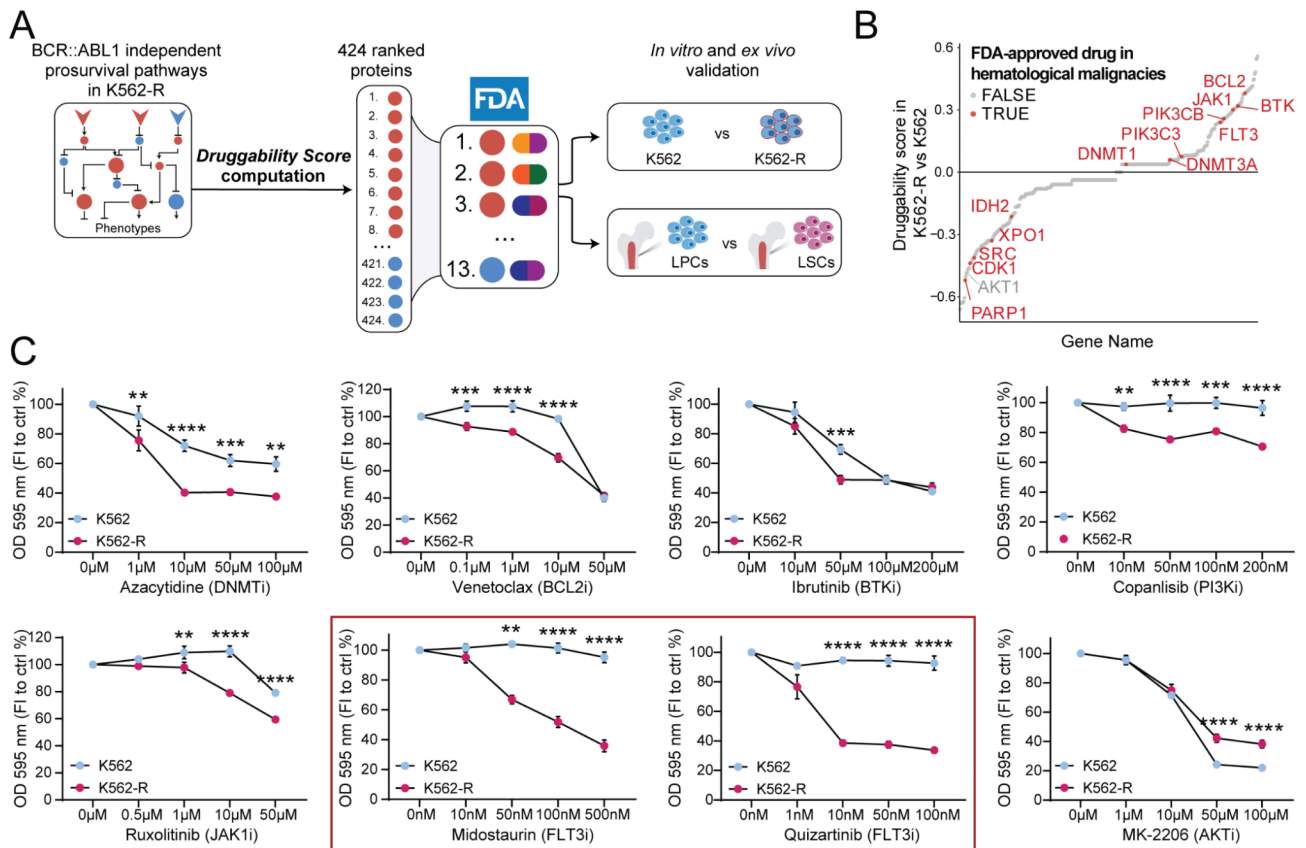


Fig. 5 Identification of new druggable targets and repurposing of FDA-approved drugs **A**. Druggable targets prioritization strategy. **B**. Scatterplot showing drug targets ranked according to the Druggability Score. **C**. MTT assay on K562 and K562-R cells exposed for 24 h at different concentrations of FDA-approved inhibitors of prioritized targets. MK-2206 (AKTi) was used as a negative control. The graphs show the percentage of absorbance at 595 nm normalized on control condition. The reported statistical significance is between K562 and K562-R cells at the same experimental condition

imatinib can inhibit unintended protein targets (off-target proteins), potentially affecting the interpretation of our signaling network analysis. To ensure the specificity of our findings, we thoroughly evaluated 13 reported imatinib off-target proteins based on three studies (Table S9) [39–41]. Our data showed that while some of these off-targets were significantly modulated at the (phospho) proteome level only in K562 or LAMA84 cells, not meeting our criteria of inclusion in the BCR::ABL1-dependent signaling network, others (e.g., DDR1, DDR2, MRLC2) were not detected in our systems. Overall, these observations suggest that our network-based approach mainly captures BCR::ABL1-specific signaling pathways, rather than broader off-target effects of imatinib.

Next, we aimed at narrowing down alternative therapeutic strategies overcoming TKI resistance and eradicating LSCs. The comparison between resistant and control cells revealed a huge remodeling of crucial processes at both the proteome and phosphoproteome regulatory layers. We integrated our data with *SignalingProfiler* 2.0 and derived the BCR::ABL1-independent signaling network. Interestingly, crucial membrane receptor kinases, including FLT3, EGFR, GRK2 and TNFR are hyperactive in the

newly generated resistant network and are potentially implicated in sustaining pro-proliferative pathways in absence of BCR::ABL1.

Thus, the generated maps not only provide a comprehensive description of the molecular mechanisms implicated in TKI-resistance, but can be leveraged to unbiasedly and systematically rank druggable targets. Indeed, we implemented the *Druggability Score*, a generally applicable algorithm which repurposes FDA-approved drugs, by prioritizing nodes, according to their topological properties and activation levels in resistant models. This strategy allowed us to pinpoint and in vitro validate BCL2, JAK1, BTK, FLT3, PI3KCB, PI3K3, DNMT1, and DNMT3A as candidate targets. Interestingly, a recent study also identified BCL2 and JAK1 as key proteins involved in TKI resistance [42], suggesting the reliability of our strategy. In our analysis, the FLT3 inhibition by two commonly used FDA approved drugs (midostaurin and quizartinib) emerged as the most effective solution to eradicate resistant cells.

FLT3 is a tyrosine-kinase receptor frequently mutated in hematological disorders and associated with dismal prognosis [43]. Remarkably, we and others observed that

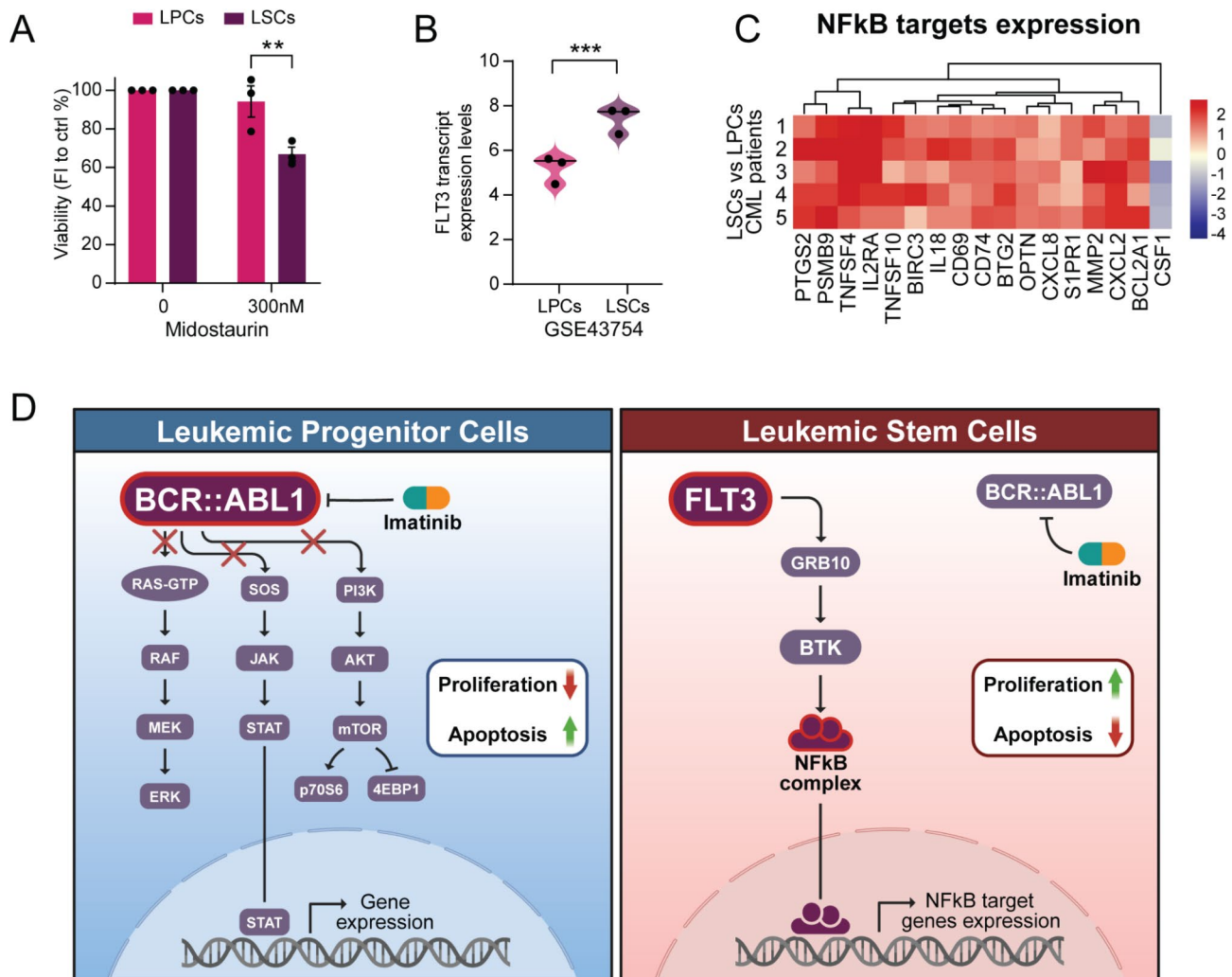


Fig. 6 LSCs rely on FLT3-NFκB axis for proliferation and survival **A**. LPCs (CD38+) and LSCs (CD26+) were sorted and exposed to midostaurin for 24 h. Viability assay was performed by trypan blue exclusion. **B**. Quantification of FLT3 in LPCs and LSCs from RNAseq analysis obtained from GEO dataset (GSE43754). **C**. Heatmap showing transcript levels of NFκB targets in LSCs compared to LPCs from RNAseq analysis obtained from GEO dataset (GSE43754). **D**. Graphic representation of how LSCs rely on the FLT3-NFκB signaling axis for proliferation and survival

FLT3 is upregulated at multiple levels in different TKI resistance models of CML: (i) protein abundance and activity in K562-R cell line; (ii) transcript level in blasts derived from an independent small cohort of TKI non-responders patients profiled in this study; (iii) transcript level in blasts derived from a large cohort of blast-phase patients [28]; and (iv) transcript level in patient-derived leukemic stem cells [27]. These observations prompted us to investigate the effect of midostaurin treatment on LSCs. Notably, pharmacological suppression of FLT3 effectively killed LSCs as compared to leukemic progenitors.

Altogether, these results indicate an acquired FLT3-dependency in resistant CML models. Mechanistically, FLT3 has been implicated in TKI resistance through the JAK-STAT axis [44]. However, we and others show that JAK suppression has a mild impact on triggering cell

death in K562-R and in patient-derived LSCs [42], suggesting alternative FLT3-mediated axes. Our results suggest the potential implication of the NFκB transcription factor in FLT3-dependent TKI resistance in leukemic stem cells.

Conclusions

Rewiring of key signaling pathways enables cancer cells to persist therapeutic treatments driving tumor progression and ultimately leading to relapse. Here we propose a novel generally applicable approach that integrates MS-based (phospho)proteomics and network-based computational pipelines. By this strategy, we generated two comprehensive maps depicting the BCR::ABL1-dependent and independent signaling networks. Notably, we discovered that therapy-resistant CML cells rely on FLT3, one of the most frequently mutated drivers of leukemia, for survival. In

conclusion, our findings provide insights into non-genetic mechanisms driving chronic myeloid leukemia resistance.

List of Abbreviations

CML	Chronic Myeloid Leukemia
LPCs	Leukemic Progenitor Cells
LSCs	Leukemic Stem Cells
MS	Mass Spectrometry
TKIs	Tyrosine Kinase Inhibitors

Supplementary Information

The online version contains supplementary material available at <https://doi.org/10.1186/s12964-025-02185-0>.

Supplementary Material 1
Supplementary Material 2
Supplementary Material 3
Supplementary Material 4
Supplementary Material 5
Supplementary Material 6
Supplementary Material 7
Supplementary Material 8
Supplementary Material 9
Supplementary Material 10

Acknowledgements

We thank Dr. Serena Paoluzi and Dr. Marta Iannuccelli for their technical support. We thank the Mass spectrometry facility at TIGEM and specifically Dr. Paolo Grumati for the support in the MS experiments.

Author contributions

Conceptualization, V.B., V.V., L.P., F.S.; resources, G.M., F.S., P.C., M.B.; software, V.V., S.G., L.P.; methodology, V.B., V.V., G.M., S.G., S.G., M.E.B., G.N., M.B., L.P., F.S.; formal analysis, V.B., V.V., G.M., S.G., P.C., M.B., D.M.; investigation, V.B., V.V., with the contribution of T.F., M.B., D.M.; writing original draft preparation, V.B., V.V., L.P., F.S.; writing review and editing, all; supervision, L.P., F.S.; funding acquisition, F.S. All authors have read and agreed to the published version of the manuscript.

Funding

This research was funded by the Italian Association for Cancer Research (AIRC) with a grant to L.P. (MFAG Grant n. 28858) and a grant to F.S. (Start-Up Grant n. 21815) and by MUR PRIN 2022 (n. E53D23004850006). G.M. is supported by MUR PRIN 2022 (n. E53D23004850006). L.P. and F.S. are supported. This study received funding from the European Union - Next- GenerationEU - National Recovery and Resilience Plan (NRRP), project P2022JRETW (FS and LP). V.V. is supported by PON-MUR fellowship (n. DOT13IEP1U-1).

Data availability

The mass spectrometry proteomics and phosphoproteomics data have been deposited to the ProteomeXchange Consortium via the PRIDE partner repository with the dataset identifier PXD056957. Patients' transcriptomic data are available on the GEO database under the ID: GSE280476. All code used for the network generation and Druggability Score analysis is available at https://github.com/SaccoPerfettoLab/Chronic_myeloid_leukemia_SignalingProfiler_2.0_analysis.

Declarations

Ethics approval and consent to participate

The study was conducted in accordance with the Declaration of Helsinki. Informed consent was obtained from all the patients.

Consent for publication

Not applicable.

Competing interests

G.N. is an advisory board member of Amplify Therapeutics. No disclosures were reported by the other authors.

Author details

- ¹Ph.D. Program in Cellular and Molecular Biology, Department of Biology, University of Rome 'Tor Vergata', Rome, Italy
- ²Department of Biology, University of Rome Tor Vergata, Rome, Italy
- ³Department of Biology and Biotechnologies "C. Darwin", University of Rome La Sapienza, Rome, Italy
- ⁴Sezione di Ematologia, Dipartimento di Scienze Radiologiche ed Ematologiche, Università Cattolica del Sacro Cuore, Roma, Italy
- ⁵Dipartimento di Scienze di laboratorio ed Ematologiche, Fondazione Policlinico A. Gemelli IRCCS, Roma, Italy
- ⁶Telethon Institute of Genetics and Medicine (TIGEM), Naples, Italy
- ⁷Department of Medical and Translational Science, Federico II University, Naples, Italy
- ⁸Scuola Superiore Meridionale (SSM), School for Advanced Studies, Genomics and Experimental Medicine program, Naples, Italy
- ⁹Department of Translational and Precision Medicine, Azienda Policlinico Umberto I, Sapienza University of Rome, Rome, Italy
- ¹⁰Health campus for Inflammation, Immunity and Infection (GC13), University of Magdeburg, Magdeburg, Germany
- ¹¹Department of Hematology, Oncology and Cell Therapy, University of Magdeburg, Magdeburg, Germany

Received: 21 January 2025 / Accepted: 30 March 2025

Published online: 10 April 2025

References

- Rowley JD. A new consistent chromosomal abnormality in chronic myelogenous leukaemia identified by quinacrine fluorescence and Giemsa staining. *Nature*. 1973;241(5405):290–3.
- Deininger MWN, Goldman JM, Melo JV. The molecular biology of chronic myeloid leukemia. *Blood [Internet]*. 2000;96(10):3343–56. Available from: <http://doi.org/10.1182/blood.V96.10.3343>
- Hochhaus A, Larson RA, Guilhot F, Radich JP, Branford S, Hughes TP, et al. Long-Term outcomes of Imatinib treatment for chronic myeloid leukemia. *N Engl J Med*. 2017;376(10):917–27.
- Hehlmann R, Lauseker M, SauBele S, Pfirrmann M, Krause S, Kolb HJ, et al. Assessment of Imatinib as first-line treatment of chronic myeloid leukemia: 10-year survival results of the randomized CML study IV and impact of non-CML determinants. *Leukemia*. 2017;31(11):2398–406.
- Jabbour E, Kantarjian H. Chronic myeloid leukemia: 2016 update on diagnosis, therapy, and monitoring. *Am J Hematol*. 2016;91(2):252–65.
- Alves R, Gonçalves AC, Rutella S, Almeida AM, Rivas JD, Las, Trougakos IP, et al. Resistance to tyrosine kinase inhibitors in chronic myeloid leukemia—from molecular mechanisms to clinical relevance. *Cancers (Basel)*. 2021;13(19):1–36.
- Patel AB, O'Hare T, Deininger MW. Mechanisms of resistance to ABL kinase Inhibition in chronic myeloid leukemia and the development of next generation ABL kinase inhibitors. *Hematol Oncol Clin North Am*. 2017;31(4):589–612.
- Ng JJ, Ong ST. Therapy Resistance and Disease Progression in CML: Mechanistic Links and Therapeutic Strategies. *Curr Hematol Malig Rep [Internet]*. 2022;17(6):181–97. Available from: <https://doi.org/10.1007/s11899-022-0067-9-z>
- Khorashad JS, Anand M, Marin D, Saunders S, Al-Jabary T, Iqbal A, et al. The presence of a BCR-ABL mutant allele in CML does not always explain clinical resistance to Imatinib. *Leukemia*. 2006;20(4):658–63.
- Sánchez R, Dorado S, Ruiz-Heredia Y, Martín-Muñoz A, Rosa-Rosa JM, Ribera J et al. Detection of kinase domain mutations in BCR::ABL1 leukemia by ultra-deep sequencing of genomic DNA. *Sci Rep [Internet]*. 2022;12(1):1–11. Available from: <https://doi.org/10.1038/s41598-022-17271-3>
- Filipek-Gorzala J, Kwieceńska P, Szade A, Szade K. The dark side of stemness—the role of hematopoietic stem cells in development of blood malignancies. *Front Oncol*. 2024;14(February):1–22.

12. Corbin AS, Agarwal A, Loriaux M, Cortes J, Deininger MW, Druker BJ. Human chronic myeloid leukemia stem cells are insensitive to Imatinib despite Inhibition of BCR-ABL activity. *J Clin Invest*. 2011;121(1):396–409.
13. Kulak NA, Pichler G, Paron I, Nagaraj N, Mann M. Minimal, encapsulated proteomic-sample processing applied to copy-number Estimation in eukaryotic cells. *Nat Methods*. 2014;11(3):319–24.
14. Humphrey SJ, Karayel O, James DE, Mann M. High-throughput and high-sensitivity phosphoproteomics with the easyphos platform. *Nat Protoc*. 2018;13(9):1897–916.
15. Tyanova S, Temu T, Sinitcyn P, Carlson A, Hein MY, Geiger T, et al. The perseus computational platform for comprehensive analysis of (prote)omics data. *Nat Methods*. 2016;13(9):731–40.
16. Liu A, Trairatphisan P, Gjerga E, Didangelos A, Barratt J, Saez-Rodriguez J. From expression footprints to causal pathways: contextualizing large signaling networks with CARNIVAL. *Npj Syst Biol Appl*. 2019;5(1):1–10.
17. Patel H, Ewels P, Peltzer A, Botvinnik O, Sturm G, Moreno D et al. nf-core/rna-seq: nf-core/rnaseq v3.12.0 - Osmium Octopus. Zenodo. 2023.
18. Ewels PA, Peltzer A, Fillinger S, Patel H, Alneberg J, Wilm A, et al. The nf-core framework for community-curated bioinformatics pipelines. *Nat Biotechnol*. 2020;38(3):276–8.
19. Dale R, Grüning B, Sjödin A, Rowe J, Chapman BA, Tomkins-Tinch CH, et al. Bioconda: sustainable and comprehensive software distribution for the life sciences. *Nat Methods*. 2018;15(7):475–6.
20. Da Veiga Leprevost F, Grüning BA, Alves Aflitos S, Röst HL, Uszkoreit J, Barsnes H, et al. BioContainers: an open-source and community-driven framework for software standardization. *Bioinformatics*. 2017;33(16):2580–2.
21. Di Tommaso P, Chatzou M, Floden EW, Barja PP, Palumbo E, Notredame C. Nextflow enables reproducible computational workflows. *Nat Biotechnol*. 2017;35(4):316–9.
22. Müller-Dott S I, Tsirovouli E, Vazquez M, Ramirez Flores R, Badia-i-Mompel P, Fallegger R, et al. Expanding the coverage of Regulons from high-confidence prior knowledge for accurate Estimation of transcription factor activities. *Nucleic Acids Res*. 2023;51(20):10934–49.
23. Venafra V, Sacco F, Peretto L. SignalingProfiler 2.0 a network-based approach to bridge multi-omics data to phenotypic hallmarks. *npj Syst Biol Appl* [Internet]. 2024;10(1). Available from: <https://doi.org/10.1038/s41540-024-00417-6>
24. Lewis M, Prouzet-Mauléon V, Lichou F, Richard E, Iggo R, Turcq B, et al. A genome-scale CRISPR knock-out screen in chronic myeloid leukemia identifies novel drug resistance mechanisms along with intrinsic apoptosis and MAPK signaling. *Cancer Med*. 2020;9(18):6739–51.
25. Sochacka-Ćwikła A, Mącznyński M, Regiec A. Fda-approved drugs for hematological malignancies—the last decade review. *Cancers (Basel)*. 2022;14(1).
26. Hamilton A, Helgason GV, Schemionek M, Zhang B, Myssina S, Allan EK, et al. Chronic myeloid leukemia stem cells are not dependent on Bcr-Abl kinase activity for their survival. *Blood*. 2012;119(6):1501–10.
27. Gerber JM, Gucwa JL, Esopi D, Gurel M, Haffner MC, Vala M, et al. Genome-wide comparison of the transcriptomes of highly enriched normal and chronic myeloid leukemia stem and progenitor cell populations. *Oncotarget*. 2013;4(5):715–28.
28. McWeeney SK, Pemberton LC, Loriaux MM, Vartanian K, Willis SG, Yochum G, et al. A gene expression signature of CD34+ cells to predict major cytogenetic response in chronic-phase chronic myeloid leukemia patients treated with Imatinib. *Blood*. 2010;115(2):315–25.
29. Soverini S, De Santis S, Monaldi C, Bruno S, Mancini M. Targeting leukemic stem cells in chronic myeloid leukemia: is it worth the effort? *Int J Mol Sci*. 2021;22(13).
30. Hallal M, Braga-Lagache S, Jankovic J, Simillion C, Bruggmann R, Uldry AC, et al. Inference of kinase-signaling networks in human myeloid cell line models by phosphoproteomics using kinase activity enrichment analysis (KAEA). *BMC Cancer*. 2021;21(1):1–15.
31. Xu X, Yin S, Ren Y, Hu C, Zhang A, Lin Y. Proteomics analysis reveals the correlation of programmed ROS-autophagy loop and dysregulated G1/S checkpoint with imatinib resistance in chronic myeloid leukemia cells. *Proteomics* [Internet]. 2022;22(1–2):e2100094. Available from: <https://pubmed.ncbi.nlm.nih.gov/34564948/>
32. Martyn GD, Veggiani G, Kusebauch U, Morrone SR, Yates BP, Singer AU, et al. Engineered SH2 domains for targeted phosphoproteomics. *ACS Chem Biol*. 2022;17(6):1472–84.
33. Reckel S, Hamelin R, Georgeon S, Armand F, Jolliet Q, Chiappe D, et al. Differential signaling networks of Bcr-Abl p210 and p190 kinases in leukemia cells defined by functional proteomics. *Leukemia*. 2017;31(7):1502–12.
34. Oliinyk D, Will A, Schneidmadel FR, Böhme M, Rinke J, Hochhaus A et al. μPhos: a scalable and sensitive platform for high-dimensional phosphoproteomics. *Mol Syst Biol* [Internet]. 2024;20(8):972–95. Available from: <https://doi.org/10.1038/s44320-024-00050-9>
35. Moreno-Lorenzana D, Avilés-Vazquez S, Sandoval Esquivel MA, Alvarado-Moreno A, Ortiz-Navarrete V, Torres-Martínez H et al. CDK1s p18INK4c and p57Kip2 are involved in quiescence of CML leukemic stem cells after treatment with TKI. *Cell Cycle* [Internet]. 2016;15(9):1276–87. Available from: <https://doi.org/10.1080/15384101.2016.1160976>
36. Popp HD, Kohl V, Naumann N, Flach J, Brendel S, Kleiner H, et al. DNA damage and Dna damage response in chronic myeloid leukemia. *Int J Mol Sci*. 2020;21(4):1–12.
37. Helgason GV, Karvela M, Holyoake TL. Kill one bird with two stones: potential efficacy of BCR-ABL and autophagy Inhibition in CML. *Blood*. 2011;118(8):2035–43.
38. Hirao T, Yamaguchi M, Kikuya M, Chibana H, Ito K, Aoki S. Altered intracellular signaling by Imatinib increases the anti-cancer effects of tyrosine kinase inhibitors in chronic myelogenous leukemia cells. *Cancer Sci*. 2018;109(1):121–31.
39. Hantschel O, Rix U, Superti-Furga G. Target spectrum of the BCR-ABL inhibitors Imatinib, nilotinib and dasatinib. *Leuk Lymphoma*. 2008;49(4):615–9.
40. Lee H, Basso IN, Kim DDH. Target spectrum of the BCR-ABL tyrosine kinase inhibitors in chronic myeloid leukemia. *Int J Hematol* [Internet]. 2021;113(5):632–41. Available from: <https://doi.org/10.1007/s12185-021-0312-6>
41. Douglass EF, Allaway RJ, Szalai B, Wang W, Tian T, Fernández-Torras A et al. A community challenge for a Pancancer drug mechanism of action inference from perturbational profile data. *Cell Rep Med*. 2022;3(1).
42. Adnan Awad S, Dufva O, Klievink J, Karjalainen E, Ianevski A, Pietarinen P et al. Integrated drug profiling and CRISPR screening identify BCR::ABL1-independent vulnerabilities in chronic myeloid leukemia. *Cell Reports Med* [Internet]. 2024;5(5):101521. Available from: <https://doi.org/10.1016/j.xcrm.2024.101521>
43. Daver N, Schlenk RF, Russell NH, Levis MJ. Targeting FLT3 mutations in AML: review of current knowledge and evidence. *Leukemia*. 2019;33(2):299–312.
44. Shin JE, Kim SH, Kong M, Kim HR, Yoon S, Kee KM et al. Targeting FLT3-TAZ signaling to suppress drug resistance in blast phase chronic myeloid leukemia. *Mol Cancer* [Internet]. 2023;22(1):1–21. Available from: <https://doi.org/10.1186/s12943-023-01837-4>
45. Perez-Riverol Y, Bai J, Bandla C, García-Seisdedos D, Hewapathirana S, Kamatchinathan S, et al. The PRIDE database resources in 2022: A hub for mass spectrometry-based proteomics evidences. *Nucleic Acids Res*. 2022;50(D1):D543–52.

Publisher's note

Springer Nature remains neutral with regard to jurisdictional claims in published maps and institutional affiliations.